

SANDIA REPORT

SAND97-2019 • UC-705

Unlimited Release

Printed August 1997

A Multi-Level Code for Metallurgical Effects in Metal-Forming Processes

Paul A. Taylor, Stewart A. Silling, Darcy A. Hughes, Douglas J. Bammann,
Michael L. Chiesa

Prepared by
Sandia National Laboratories
Albuquerque, New Mexico 87185 and Livermore, California 94550

Sandia is a multiprogram laboratory operated by Sandia
Corporation, a Lockheed Martin Company, for the United States
Department of Energy under Contract DE-AC04-94AL85000.

Approved for public release; distribution is unlimited



Sandia National Laboratories

Issued by Sandia National Laboratories, operated for the United States Department of Energy by Sandia Corporation.

NOTICE: This report was prepared as an account of work sponsored by an agency of the United States Government. Neither the United States Government nor any agency thereof, nor any of their employees, nor any of their contractors, subcontractors, or their employees, makes any warranty, express or implied, or assumes any legal liability or responsibility for the accuracy, completeness, or usefulness of any information, apparatus, product, or process disclosed, or represents that its use would not infringe privately owned rights. Reference herein to any specific commercial product, process, or service by trade name, trademark, manufacturer, or otherwise, does not necessarily constitute or imply its endorsement, recommendation, or favoring by the United States Government, any agency thereof or any of their contractors or subcontractors. The views and opinions expressed herein do not necessarily state or reflect those of the United States Government, any agency thereof or any of their contractors.

Printed in the United States of America. This report has been reproduced directly from the best available copy.

Available to DOE and DOE contractors from
Office of Scientific and Technical Information
PO Box 62
Oak Ridge, TN 37831

Prices available from (615) 576-8401, FTS 626-8401

Available to the public from
National Technical Information Service
US Department of Commerce
5285 Port Royal Rd
Springfield, VA 22161

NTIS price codes
Printed copy: A08
Microfiche copy: A01

A Multi-Level Code for Metallurgical Effects in Metal-Forming Processes

Paul A. Taylor and Stewart A. Silling
Computational Physics and Mechanics Department

Sandia National Laboratories
P.O. Box 5800
Albuquerque, NM 87185-0820

Darcy A. Hughes
Materials Reliability Department

Douglas J. Bammann and Michael L. Chiesa
Solid and Material Mechanics Department

Sandia National Laboratories
P.O. Box 969
Livermore, CA 94551-0969

Abstract

We present the final report on a Laboratory-Directed Research and Development (LDRD) project, *A Multi-Level Code for Metallurgical Effects in Metal-Forming Processes*, performed during the fiscal years 1995 and 1996. The project focused on the development of new modeling capabilities for simulating forging and extrusion processes that typically display phenomenology occurring on two different length scales. In support of model fitting and code validation, ring compression and extrusion experiments were performed on 304L stainless steel, a material of interest in DOE nuclear weapons applications.

Acknowledgments

The authors would like to thank the following people: Mr. R. Bell for the development and implementation of the moving subgrid scheme, Mr. J. Totten for his execution of the ring compression experiments, Mr. N. Bhatena, of Wyman-Gordon Forgings, in conducting the extrusion experiments, Mr. H. Hsiung for his assistance in the metallurgical analysis of the extrusion samples, and Ms. M. Chen for her assistance in data digitizing and image scanning.

Contents

1. Introduction.....	7
2. Computer Code Enhancements.....	9
2.1. Multi-Grid Scheme in CTH/EPIC	9
2.2. Dynamic Relaxation Algorithm.....	10
2.3. Viscoplasticity Constitutive Model	10
2.4. Friction Model	12
3. Experimental Results	13
3.1. Ring Compression Experiments	13
3.2. Extrusion Experiments.....	15
4. Fitting and Validation	21
4.1. Friction Model Fitting.....	21
4.2. Code Validation	21
5. Summary	23
References.....	25
Appendix A. Moving Subgrid Option	27
Appendix B. Dynamic Relaxation Algorithm	29
B.1. DR for Equilibrium Problems	29
B.2. DR for Quasi-static Problems	30
B.3. Application of Loads.....	33
B.4. Convergence Test.....	33
B.5. Choice of Damping Coefficient	34
B.6. Constitutive Modeling Issues	35
B.7. Code Modification Steps.....	35

Figures

2.1. Eulerian/Lagrangian description of forging problem with Eulerian subgrids	9
2.2. (a)-Initial configuration and (b)-equivalent plastic strain plot at 7 sec. into extrusion simulation using CTH/EPIC and the dynamic relaxation technique ..	11
2.3. Graphic description of Anand's friction model for metal-forming	12
3.1. Schematic of ring compression experiment.....	13
3.2. Ring compression data for 304L stainless steel at 800°C.....	14
3.3. Ring compression data for 304L stainless steel at 1000°C.....	14
3.4. Schematic diagram of the extrusion experiments	15
3.5. Optical micrograph and corresponding plastic shear strain distribution for upper section of extrusion specimen 1 (specimen radius ~ 3.1 mm).....	17
3.6. Optical micrograph and corresponding plastic shear strain distribution for middle section of extrusion specimen 1 (specimen radius ~ 3.1 mm).....	18
3.7. Optical micrograph and corresponding plastic shear strain distribution for lower section of extrusion specimen 1 (specimen radius ~ 3.1 mm).....	19
A.1. Graphical representation of moving subgrid option	27
B.1. Solution of an equilibrium problem by DR. Time evolutions of the load and the total kinetic energy of the mesh are shown.....	31

B.2. Solution of a quasi-static problem by DR	32
---	----

1. Introduction

This report summarizes the work performed for the Laboratory-Directed Research and Development (LDRD) project, *A Multi-Level Code for Metallurgical Effects in Metal-Forming Processes*.

The objective of this project was the development of a multi-level computational method to predict the final thermomechanical state of a material that has undergone a forging or extrusion process. Typically, in such a process, there exist localized regions, or “boundary layers,” of the workpiece that are in close proximity to the tooling hardware and, as a consequence, experience significantly greater temperature gradients and strains than material somewhat removed from the workpiece/tooling interface. Therefore, the simulation method must be able to predict both (1) the overall bulk flow of the workpiece material and (2) the microscale effects that occur in the boundary layer of the workpiece near the interface between it and the tooling hardware.

In order to accurately simulate forging and extrusion processes, we have developed a multi-grid method that would predict and couple the thermomechanical responses of the workpiece in two distinct length-scale regimes: the bulk flow regime, and the boundary layer regime in which the characteristic length scale can be on the order of $1/10$ to $1/100$ of that characteristic of the bulk flow regime. This scheme was incorporated into a coupled Eulerian/Lagrangian code in which the workpiece response could be modeled in an Eulerian grid and the tooling hardware modeled using Lagrangian finite element methods. Eulerian grid subdomains of high resolution are used to model the phenomena occurring in the boundary layer of the workpiece, the solution of which is then coupled to the hybrid Eulerian/Lagrangian calculation to predict the overall material flow of the workpiece.

The codes chosen for the Eulerian/Lagrangian coupling are the solid dynamics codes, CTH [1] and EPIC [2]. The linking of CTH and EPIC is accomplished using the driver code, Zapotec [3]. Zapotec employs a hybrid Eulerian/Lagrangian solution methodology [4] in which soft material is treated in an Eulerian framework and hard material is modeled with a Lagrangian code.

The solid dynamics code CTH is an Eulerian code that explicitly solves the finite-difference analogs for the equations of momentum and energy balance; whereas, EPIC is a Lagrangian finite element code that also employs an explicit time integration scheme to solve the equations of momentum and energy balance. As such, both of these codes employ the Courant criterion that restricts the size of the time step taken at each iteration to ensure the stability of their numerical solutions. This feature in the codes imposes a significant restriction on the applicability of the CTH/EPIC coupled code to problems of forging and extrusion. In particular, the CTH/EPIC coupled code with its explicit time integration schemes is well suited to treating solid dynamics problems that occur on microsecond to millisecond time scales whereas, forging and extrusion processes typically occur on a time scale of 0.1 to 10 seconds. Early attempts to use CTH/EPIC to simulate a forging or extrusion process required simulation times on the order of a hundred microseconds, which gave rise to unacceptable consequences due to material inertia and strain rate effects.

Consequently, another aspect of the LDRD project was the development and implementation of a time integration scheme based on the dynamic relaxation method [5]. This approach allows us to avoid the adverse consequences of the timestep constraints inherent in CTH and EPIC and permits the simulation of quasi-static processes such as forging and extrusion.

In order to represent the complex temperature-dependent plastic flow of the workpiece, a sophisticated viscoplasticity model is required. Consequently, another task of the LDRD project was the implementation and testing of the Bammann-Chiesa-Johnson (BCJ) viscoplastic/damage model [6,7]. This model describes the deviatoric elastic-viscoplastic response of metals at temperatures below melt and the cumulative damage resulting from ductile void growth.

Representation of the friction forces between the workpiece and the tooling hardware required us to adopt an accurate friction model relevant to metal forming applications. In particular, the friction model developed by Anand and Tong [8] was implemented into the CTH/EPIC code and fitted to ring compression data collected for the project.

For the purposes of model fitting and code validation, we selected 304L stainless steel as a candidate material which is of particular interest in DOE nuclear weapons applications. In order to fit the friction model implemented for the project, we conducted ring compression experiments on 304L stainless steel at the elevated temperatures typical of forging and extrusion operations for this material. For the purpose of validating our simulation method, we also conducted extrusion experiments and subsequent metallurgical analyses on samples of 304L stainless steel to determine the resulting internal plastic flow field of the samples. Validation then becomes a matter of comparing the experimentally determined plastic flow field, as induced by the extrusion process, and its prediction by means of numerical simulation.

2. Computer Code Enhancements

2.1 Multi-Grid Scheme in CTH/EPIC

In general, forging and extrusion problems involve soft and hard materials (viz., workpiece and tooling hardware), interacting with each other. The workpiece material tends to undergo large strains; whereas, the tooling hardware experiences small strains and usually remains elastic in its response. The application of Eulerian/Lagrangian methods to forging/extrusion problems brings with it two distinct advantages over strictly Eulerian or Lagrangian methods. First, the Eulerian portion can track the flow of the workpiece without concern for mesh entanglement, and the Lagrangian finite element representation of the tooling hardware provides a fast calculation of its material response. Secondly, by overlaying the Eulerian mesh to include the tooling hardware boundaries, we have a well-defined interface at which friction and heat transfer models can be applied.

In many forging/extrusion applications, the friction and heat transfer that occur at the interfaces between the workpiece and tooling hardware give rise to significantly greater plastic strains and temperature gradients in a “boundary layer” located within the workpiece adjacent to the material interface. In order to efficiently resolve the phenomena occurring in the boundary layer, we have developed a multi-grid scheme that overlays an Eulerian subgrid of much finer resolution than that which tracks the bulk response of the workpiece material (see Figure 2.1). By defining mesh cell dimensions of much finer size in the subgrids, we can model the thermomechanical response of the workpiece in the boundary layer with greater resolution.

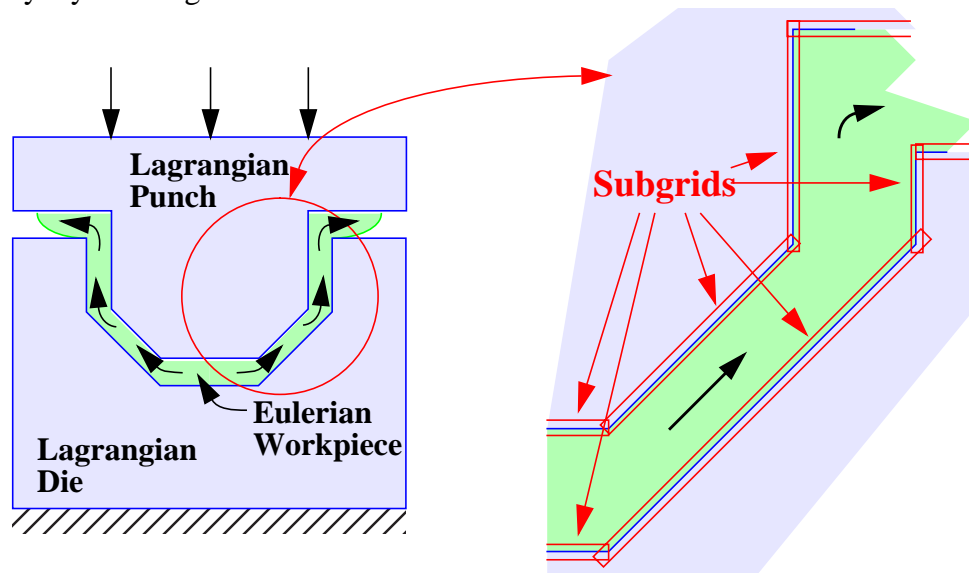


Figure 2.1. Eulerian/Lagrangian description of forging problem with Eulerian subgrids.

In order to be useful, the Eulerian subgrids must be able to move along with and track the material interfaces. This is achieved by identifying each subgrid with a Lagrangian tracer point, i.e., a point that is originally fixed in one of the materials in close proximity to the

interface and moves along with that material. Further details of this scheme as it is implemented in CTH can be found in Appendix A.

2.2 Dynamic Relaxation Algorithm

The codes selected for our Eulerian/Lagrangian methodology are the Eulerian finite difference code CTH [1] and the Lagrangian finite element code, EPIC [2]. As mentioned previously, these codes are well suited to solving various solid dynamics problems and were not originally intended to simulate low strain-rate processes. Since the majority of forging and extrusion processes involve low strain-rates, we needed to implement a time integration scheme in CTH and EPIC that would relax the time step controls used by the codes so that these processes could be simulated. The scheme we adopted is based on the dynamic relaxation (DR) technique [5] which is used with solid dynamics codes to solve equilibrium or quasi-static problems in continuum and structural mechanics. The specifics on the technique and its implementation into solid dynamics computer codes is outlined in greater detail in Appendix B.

A sample extrusion simulation, represented in Figure 2.2, demonstrates the CTH/EPIC coupled code employing the dynamic relaxation algorithm. In the figure, the extrusion punch and die are represented by the finite element meshes and the workpiece billet is extruded partially through the die over a period of 7 seconds. The problem geometry is axisymmetric (about the $X=0$ axis) with the tooling hardware modeled as S-7 tool steel and the workpiece as copper at 800°C . The figure displays only half of the tooling hardware whereas the workpiece is fully shown. In Figure 2.2b, the apparent “liner” around the workpiece is an artifact of the graphics software displaying the problem and the coupled Eulerian/Lagrangian methodology of the Zapotec code.

2.3 Viscoplasticity Constitutive Model

During a forging or extrusion process, the workpiece can undergo a complex history of deformation at elevated temperatures. Typically, the response of the workpiece material will be a result of strain hardening, strain rate effects, and thermal softening. The strain hardening can be due to a combination of isotropic and kinematic hardening. Consequently, the need exists for an advanced plasticity model that can capture these effects if one hopes to accurately simulate forging and extrusion processes.

We have implemented the Bammann-Chiesa-Johnson (BCJ) [6,7] viscoplastic/damage model into the CTH/EPIC code to describe the response of the workpiece material. In particular, the model describes the deviatoric elastic-viscoplastic response of metals and the cumulative damage resulting from ductile void growth. The viscoplastic response of the model incorporates isotropic and kinematic hardening as well as strain rate and thermal effects. Damage modeling is based on an analytic expression for spherical void growth. The damage growth rate is dependent on the effective stress, tensile pressure, plastic strain rate, and the current damage level. The deviatoric response of the model is dependent on the damage in such a way as to locally degrade elastic moduli and concentrate plastic flow. A

complete description of the BCJ model, its implementation into the code, and a simulation exemplifying the model is described in a separate Sandia report [9].

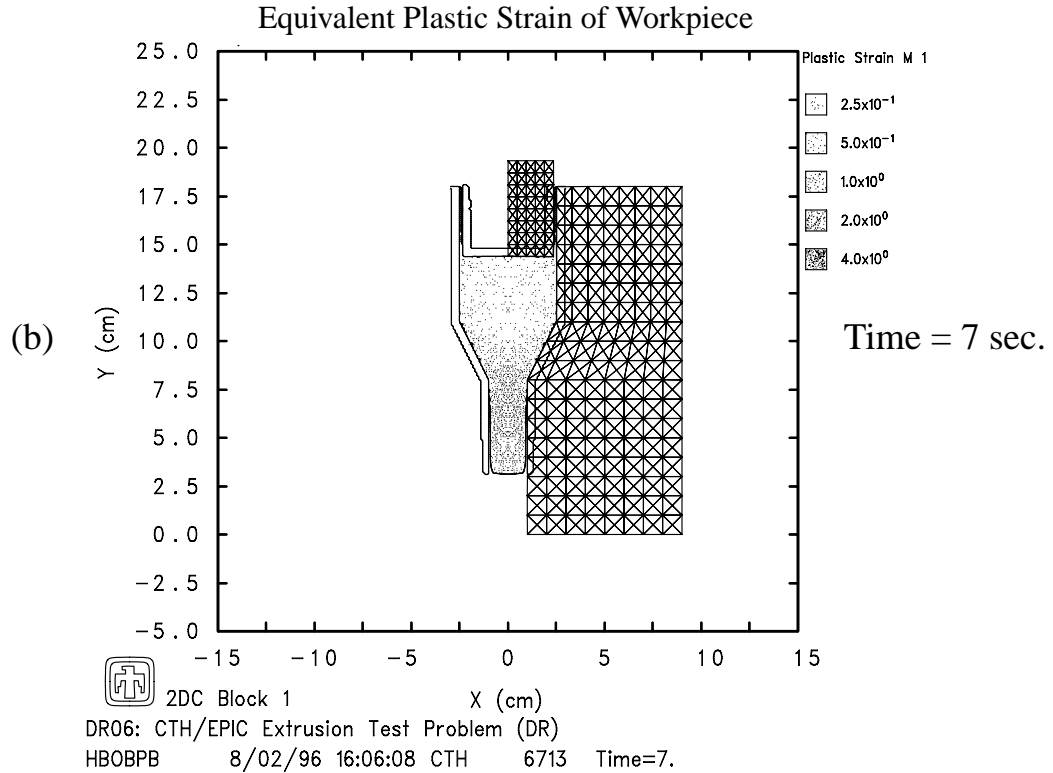
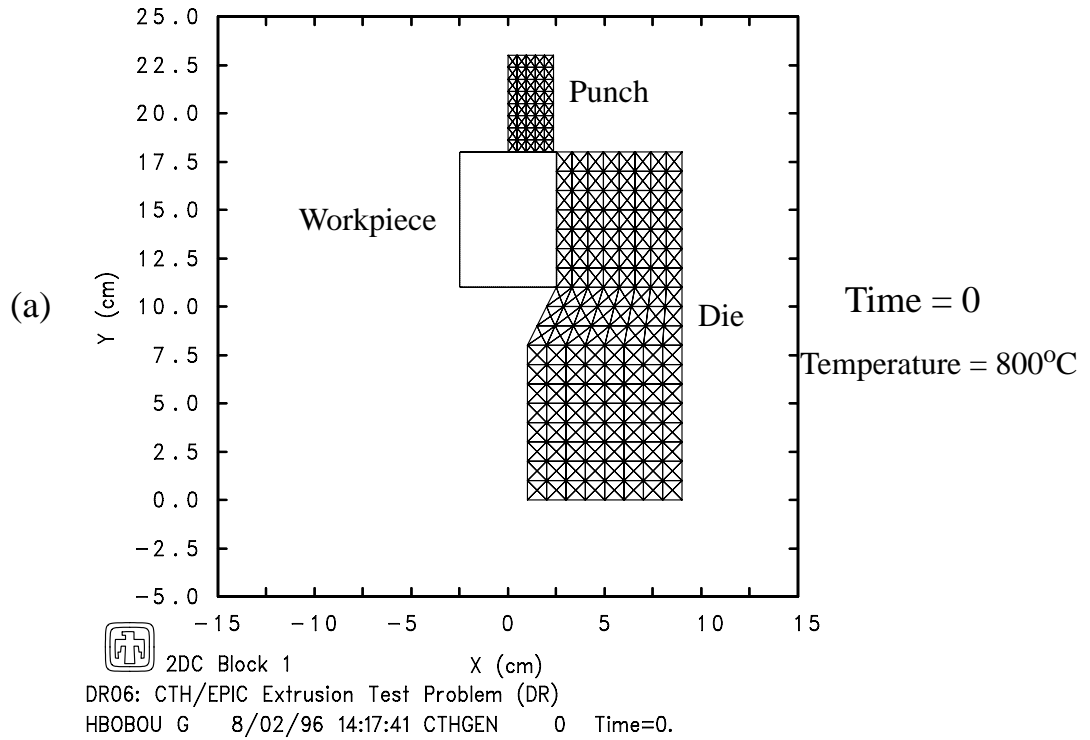


Figure 2.2. (a)-Initial configuration and (b)-equivalent plastic strain plot at 7 seconds into extrusion simulation using CTH/EPIC and the dynamic relaxation technique.

2.4 Friction Model

In order to describe the friction forces that exist at the interface between the workpiece material and tooling hardware, we have implemented an advanced friction model that has been proposed by Anand and Tong [8] specifically for metal-forming applications. The friction model defines the relation between the resultant shear stress τ at a material interface and its associated normal stress resultant σ according to the relation

$$\tau = \tau^{\infty} \tanh\left(\frac{\mu\sigma}{\tau^{\infty}}\right), \quad (2.1)$$

where τ^{∞} is the asymptotic value of τ for large values of σ , and μ is the coefficient of friction for low values of σ . A graphical description of the friction model is depicted in Figure 2.3.

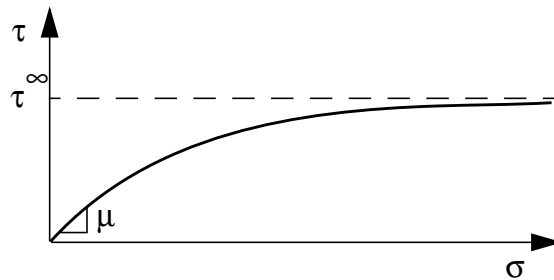


Figure 2.3. Graphic description of Anand's friction model for metal-forming.

The friction model is implemented in the Zapotec [3] driver code that couples CTH and EPIC to treat solid dynamics problems using the hybrid Eulerian/Lagrangian solution methodology.

3. Experimental Results

3.1 Ring Compression Experiments

This section describes the ring compression experiments that were conducted at elevated temperatures in order to fit the friction model (see e.g., [10]), outlined in section 2.4, to describe the interfacial stresses that will be encountered in the extrusion experiments on 304L stainless steel. Ring compression tests are typically performed in order to determine the interfacial friction stresses that exist between the ring specimen and the tooling hardware, or platens, that compress the specimen axially to a predetermined extent (see Figure 3.1). The amount of friction that exists between the ring specimen and the platens is reflected by the extent of change in the inside diameter of the ring. (Little or no friction results in an increase of the inside diameter during compression, whereas a large amount of friction results in a decrease of the inside diameter). For model fitting purposes, useful ring compression data typically assumes the form of “decrease in inner diameter” as a function of “reduction in thickness.”

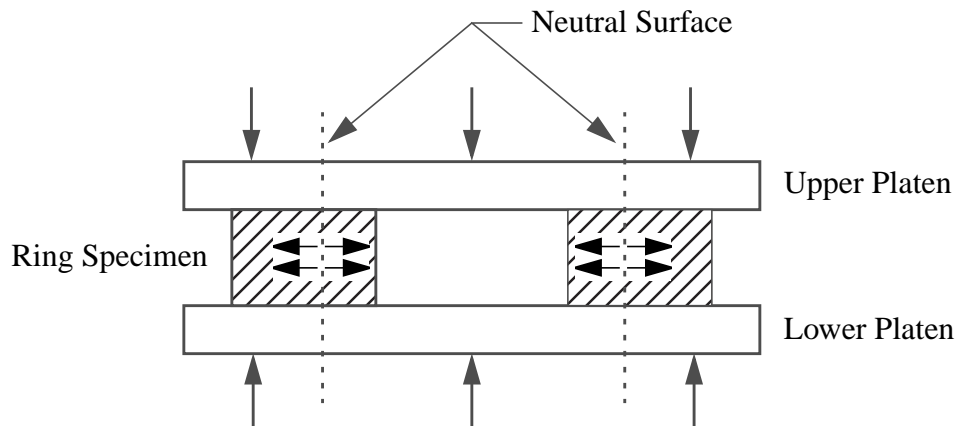


Figure 3.1. Schematic of ring compression experiment.

Ring compression experiments and the resulting friction data can be obtained for either dry or lubricated samples. Since the extrusion experiments, performed for code validation purposes and described in section 3.2, involve lubrication, we have conducted our ring compression experiments using the same lubricant employed in those extrusions.

In our ring compression experiments, the specimen geometry was that of a hollow circular cylinder (or disk) with an inside diameter of 1.016 cm, an outside diameter of 2.032 cm, and an axial thickness of 0.6782 cm. The samples were placed between flat platens consisting of either the Inconel X-750 alloy (for experiments at 800°C) or a Si_3N_4 ceramic (for experiments at 1000°C).

The ring compression experiments subjected the 304L stainless steel ring samples to axial compressions of up to roughly a 60% reduction in thickness for two different temperatures, namely, 800°C and 1000°C. There were 20 ring compression experiments conducted at 800°C and 16 experiments conducted at 1000°C. The experimental results for the ring

compression tests at 800°C and 1000°C are presented in Figures 3.2 and 3.3 respectively. The existence of the low data point (at 48% reduction in thickness) in Figure 3.3 can be attributed to the loss of lubrication during the associated experiment. Consequently, this point was ignored in the fitting of the friction model as described later in section 4.1.

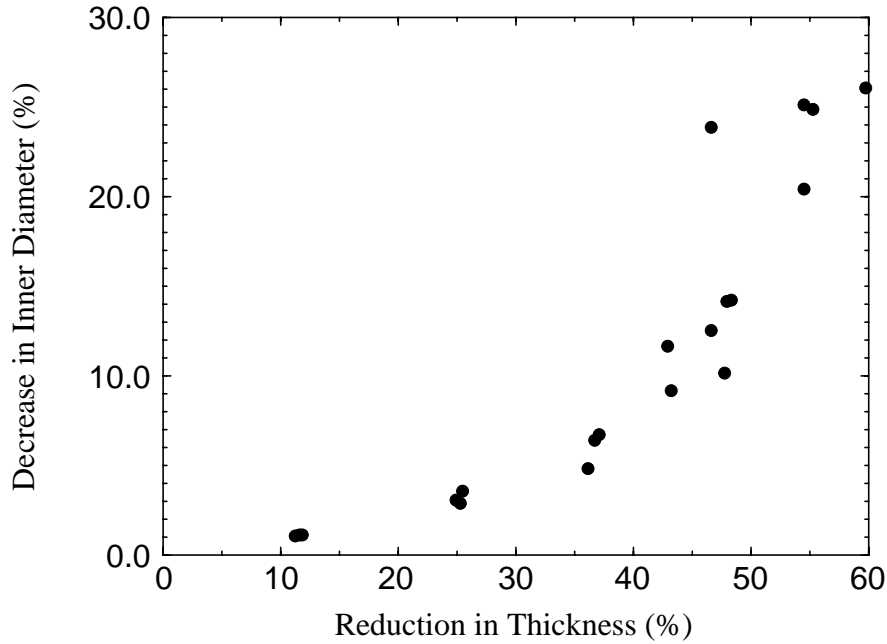


Figure 3.2. Ring compression data for 304L stainless steel at 800°C.

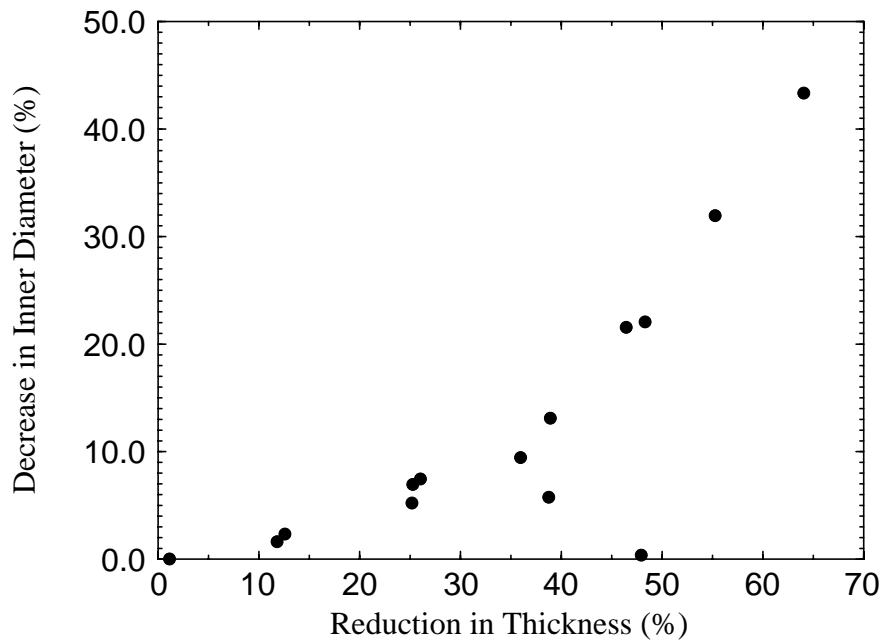


Figure 3.3. Ring compression data for 304L stainless steel at 1000°C.

3.2 Extrusion Experiments

In order to validate our simulation method, extrusion experiments were performed on 304L stainless steel samples containing ferrite stringers. These stringers, initially oriented perpendicular to the longitudinal axis of each specimen, are re-oriented during the extrusion process reflecting the internal plastic flow field of the specimen. Subsequent metallurgical analyses were performed on sections of the extruded specimens to determine stringer orientations throughout the specimen. Using a simple relation between change in stringer orientation and shear strain, we were able to determine the plastic shear strain distributions throughout each specimen.

In the experiments, cylindrical samples of 304L stainless steel were extruded, under isothermal conditions, through a reduction die to 25% of the sample's original diameter (see Figure 3.4).

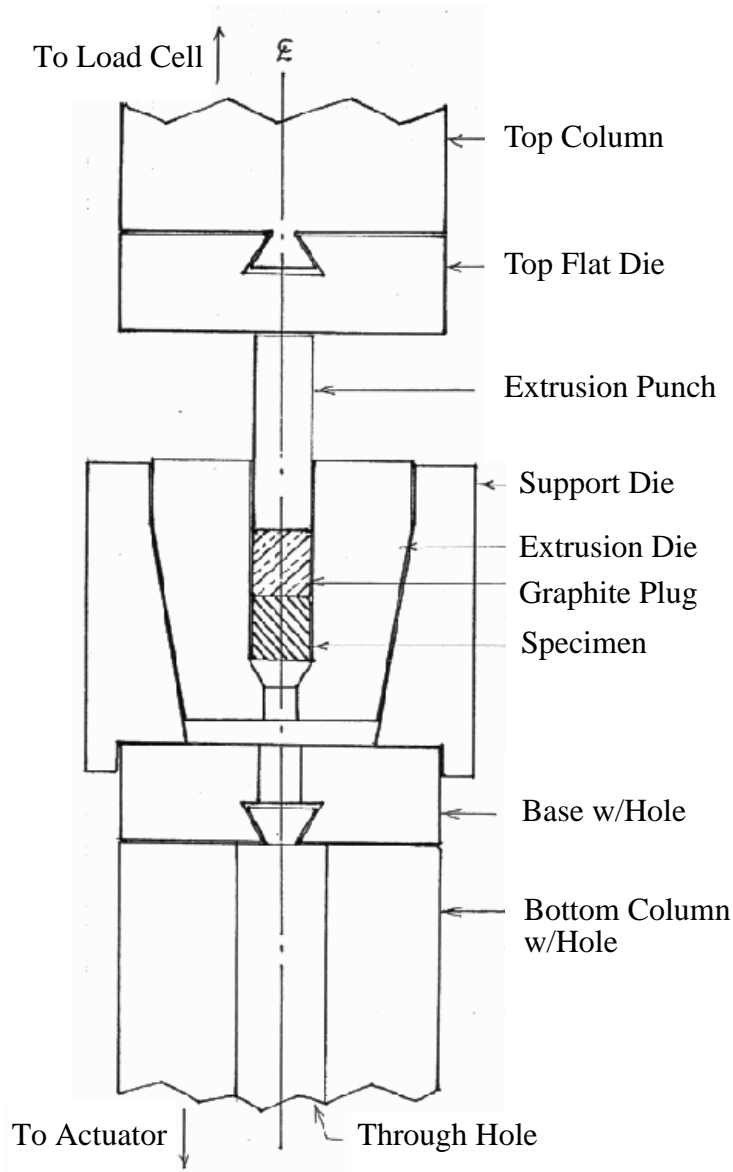


Figure 3.4. Schematic diagram of the extrusion experiments.

The extrusion experiments were performed at the Wyman-Gordon Forgings Company, Houston, Texas, under the direction of Mr. Noshir Bhathena. Four extrusions were conducted for the project; the first three under identical conditions and the fourth at a higher ram speed and hence, higher strain rate. The conditions of the experiments were as follows:

Sample composition: 304L stainless steel

Temperature: 1037°C (isothermal conditions: both sample and tooling hardware)

Initial sample geometry: cylindrical, 1.27 cm diameter, 1.27 cm long

Final sample geometry: cylindrical, 0.635 cm diameter, ~5 cm long

Lubricant: glass-based (proprietary information of Wyman-Gordon)

Tooling composition: super alloy (proprietary information of Wyman-Gordon)

Die angle: 60°

Die throat diameter: 0.635 cm

Ram Speed: 0.13 cm/min (experiments 1-3), 1.4 cm/min (experiment 4)

Nominal strain rate: 0.01/sec (experiments 1-3), 0.10/sec (experiment 4)

The shear strain distribution data from the low strain rate experiments 1-3 are fairly consistent whereas the data from the higher strain rate experiment 4 is incomplete due to the lack of ferrite stringer image data in the upper 1/3 of the specimen. However, the strain distribution in the remainder of specimen 4 suggests little difference between the results of experiments 1-3 and those of experiment 4, which was conducted at the higher ram speed.

Figures 3.5, 3.6, and 3.7 display the plastic shear strain distributions in the upper, middle, and lower thirds of the extrusion specimen from experiment 1 along with the corresponding optical micrographs of the specimen's cross-section. The micrographs were used to determine the strain distributions by tracking the reorientation of the ferrite stringers, which appear as dark lines in the micrographs. Note also, the concave shape at the top of the upper section of the specimen in Figure 3.5. This feature is a result of "suck-in," a term used in the forging industry to describe the process of material being drawn in towards the center of the specimen as a result of extrusion process. Suck-in was observed in all four extrusion experiments.

Error bars are included in the shear strain distribution plots, which are a result of the uncertainty of measuring the angles through which the ferrite stringers rotated. As can be seen in all three sections, the plastic shear strain increases exponentially from a value of zero at the center of the specimen to values ranging from 10 to 50 at the maximum radial distance of the specimen. Furthermore, this radial dependence of the plastic shear strain appears qualitatively similar for all three sections.

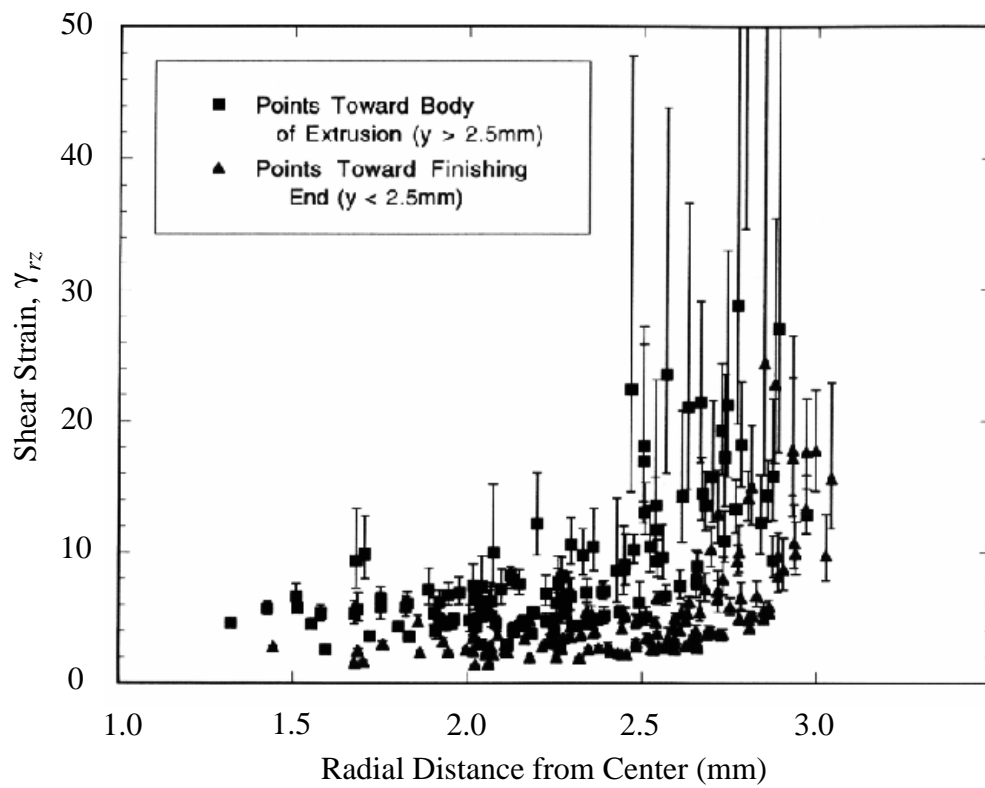
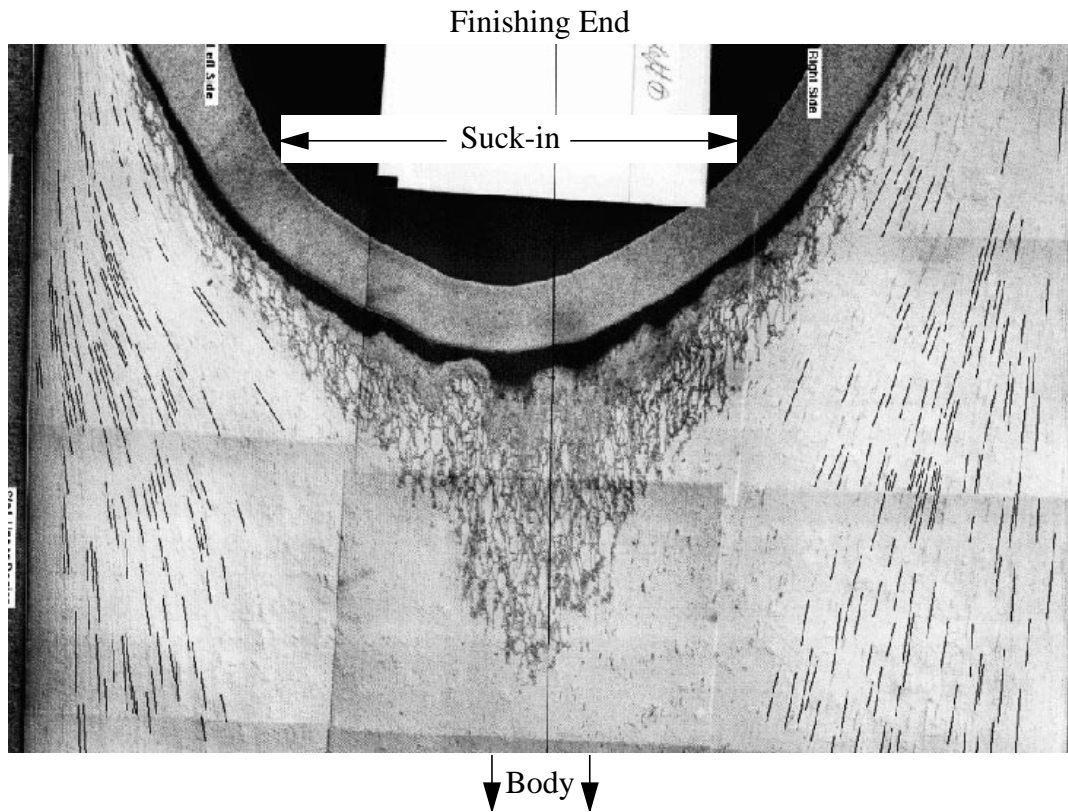


Figure 3.5. Optical micrograph and corresponding plastic shear strain distribution for upper section of extrusion specimen 1 (specimen radius ~ 3.1 mm).

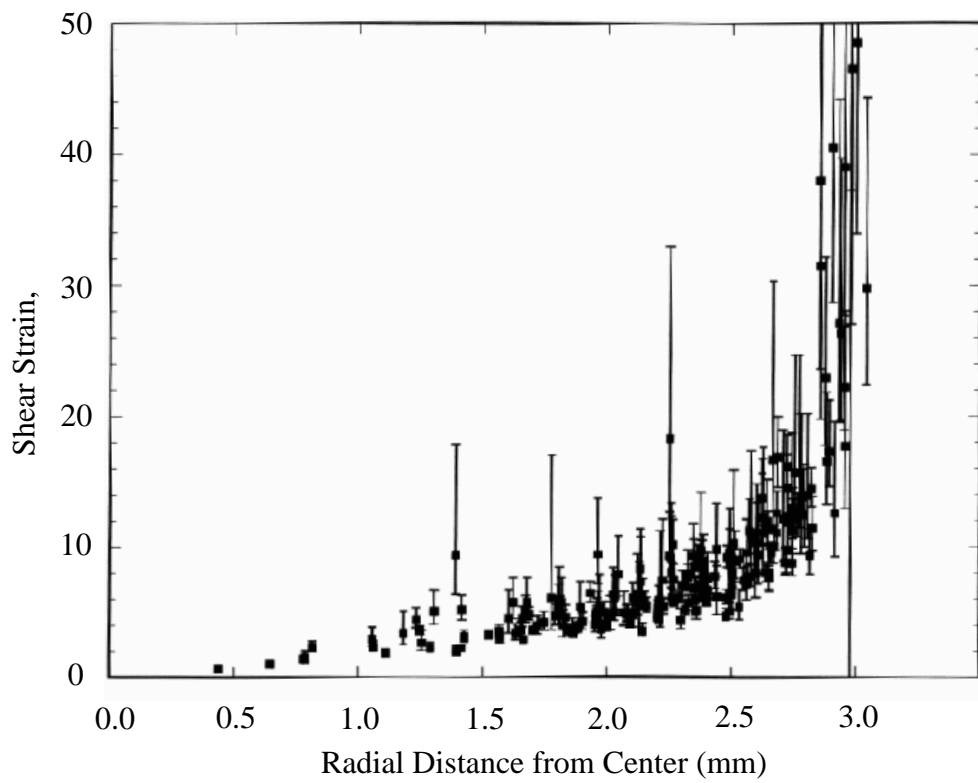
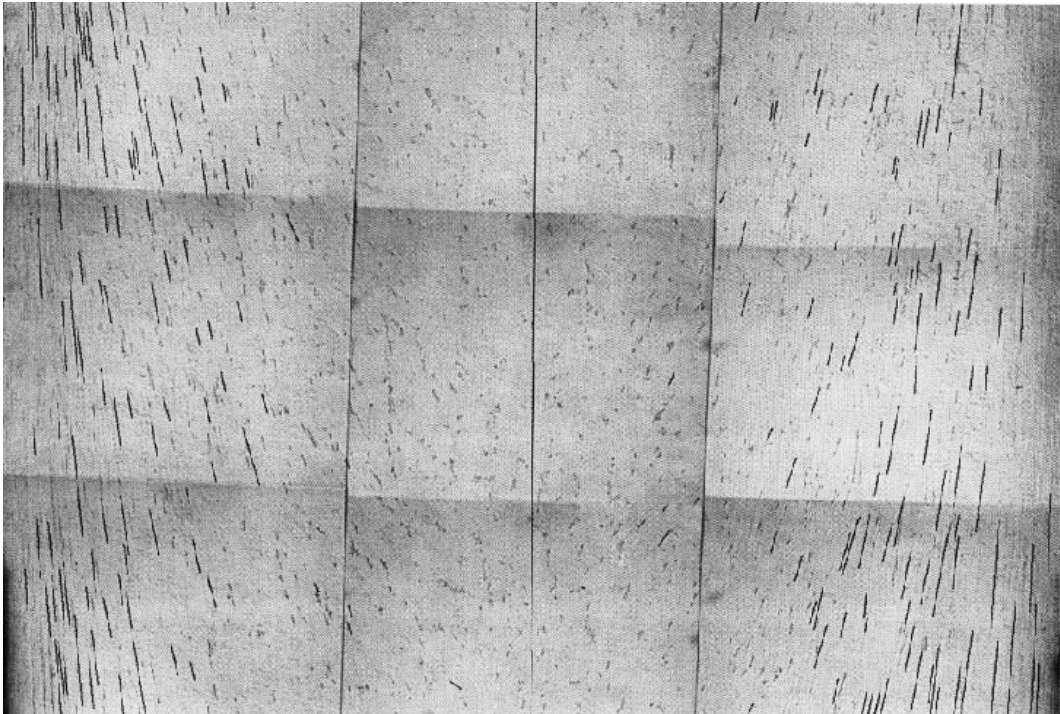


Figure 3.6. Optical micrograph and corresponding plastic shear strain distribution for middle section of extrusion specimen 1 (specimen radius ~ 3.1 mm).

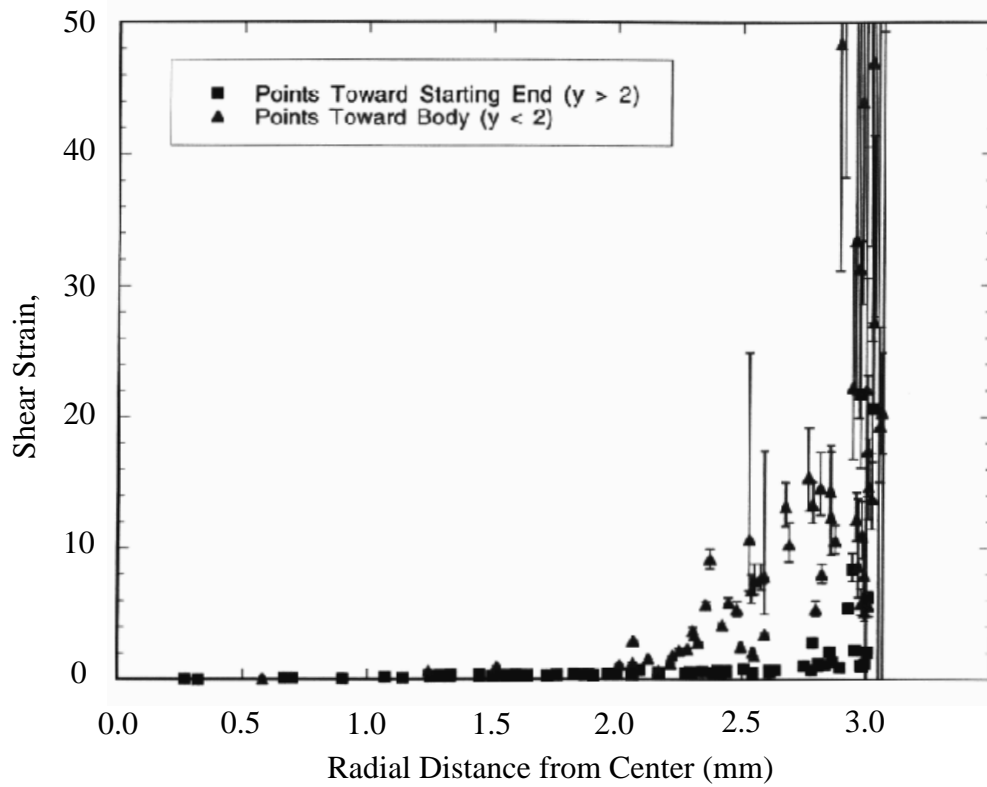
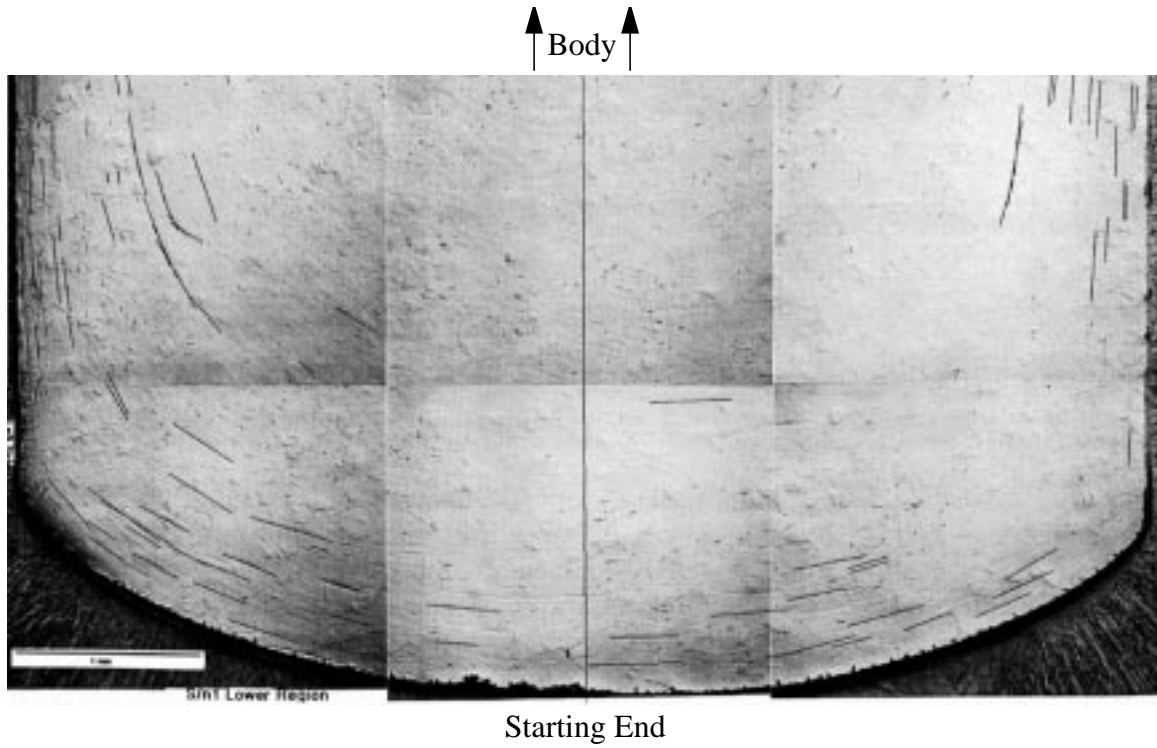


Figure 3.7. Optical micrograph and corresponding plastic shear strain distribution for lower section of extrusion specimen 1 (specimen radius ~ 3.1 mm).

Intentionally Left Blank

4. Fitting and Validation

4.1 Friction Model Fitting

The process of fitting the friction model was one of trial-and-error and performed by simulating the ring compression experiments (described in section 3.1) numerically, employing Anand’s friction model, and incrementally changing the model parameters to achieve a “best fit” to the experimental data. Since the temperature conditions of the 1000°C experiments were more closely related to those of the extrusion experiments (described in section 3.2) intended for code validation purposes, the friction model was fitted using the 1000°C experimental results.

As a result of the fitting process, the following form for the friction model most accurately captures the ring compression data, as depicted in Figure 3.3:

$$\tau = \tau^{\infty} \tanh\left(\frac{\mu\sigma}{\tau^{\infty}}\right), \quad (4.1)$$

$$\tau^{\infty} = \frac{m\bar{\sigma}}{\sqrt{3}}, \quad m = 0.35, \quad \text{and} \quad \mu = 0.175, \quad (4.2)$$

where $\bar{\sigma}$ is the equivalent von Mises flow stress of the workpiece material. This model for friction was made available in the CTH/EPIC coupled code by means of its implementation into the driver code, Zapotec [3], which links and interfaces CTH and EPIC to create a coupled Eulerian-Lagrangian analysis.

4.2 Code Validation

As mentioned throughout this report, the extrusion experiments, described in section 3.2, were conducted in order to validate our simulation method developed for the LDRD project. However, the validation phase of the simulation method, that is, exercising all of the software enhancements that we have described in chapter 2 from a single software package, has not yet been completed and as such, will not be included in this final report. It is our intent to complete this phase of the work in a follow-on effort which has been funded under the Accelerated Strategic Computing Initiative (ASCI) program at Sandia Laboratories.

Intentionally Left Blank

5. Summary

In this report, we have described a method that is intended to provide a simulation capability to accurately model forging and extrusion processes. Typically, these processes involve thermomechanical phenomena occurring on multiple length scales. We have used a computational platform that employs a hybrid Eulerian-Lagrangian analysis as the baseline modeling technique. Several new capabilities were implemented in the baseline simulation method under this project. In particular, we have implemented:

1. A dynamic relaxation algorithm that permits us to simulate forging and extrusion processes on long time scales.
2. A multi-grid scheme to simulate the thermomechanical response of materials on different spatial length scales.
3. The Bammann-Chiesa-Johnson (BCJ) constitutive model describing viscoplasticity and damage accumulation as it occurs in the workpiece material.
4. An advanced friction model specifically designed to describe the interfacial stresses that exist between the workpiece and tooling hardware.

Furthermore, we have conducted:

5. Ring compression experiments on lubricated samples of 304L stainless steel at temperatures that are typical of forging and extrusion operations for this material.
6. Calibration of the friction model using the ring compression data to define the workpiece/tooling interactions that will exist in the subsequent extrusion experiments performed on 304L stainless steel.
7. Extrusion experiments on samples of 304L stainless steel and subsequent metallurgical analyses on cross-sections of the extruded samples. From these analyses, we have determined the internal plastic flow fields of the samples that were induced by the extrusion process. This data is used for validation purposes by comparing the experimentally determined plastic flow fields, as induced by the extrusion process, and their prediction by means of simulation.

The validation phase of the project, however, has not yet been completed and as such, will not be included in this final report. It is our intent to complete this phase of the work and document the results in a forthcoming report. Follow-on funding has been secured for this purpose.

Intentionally Left Blank

References

- [1] J. M. McGlaun, S. L. Thompson, L. N. Kmetyk, and M. G. Elrick, "A Brief Description of the Three-Dimensional Shock Wave Physics Code CTH," Sandia National Laboratories report SAND89-0607 (1990).
- [2] G. R. Johnson, R. A. Stryk, T. J. Holmquist, and S. R. Beissel, "User Instructions for the 1996 Version of the EPIC Code," Alliant Techsystems Inc., Hopkins, Minnesota, March 1996.
- [3] J. K. Prentice, "A Methodology for Performing Coupled Eulerian/Lagrangian Solid Dynamics Hydrocode Calculations," in preparation.
- [4] J. K. Prentice, "Methodology and Applications of the Hull Hydrocode Eulerian/Lagrangian Link," in *Shock Waves in Condensed Matter-1987*, S. C. Schmidt and N. C. Holmes, eds., pp. 219-222, North-Holland Physics Publishing (1988).
- [5] P. Underwood, "Dynamic Relaxation," in *Computational Methods for Transient Analysis*, T. Belytschko and T. J. R. Hughes, eds., Elsevier Science Publishers B.V., pp. 245-265 (1983).
- [6] D. J. Bammann, M. L. Chiesa, M. F. Horstemeyer, and L. I. Weingarten, "Failure in Ductile Materials using Finite Element Methods," in *Structural Crashworthiness and Failure*, eds. N. Jones, and T. Wierzbicki, Elsevier Applied Science, 1 (1993).
- [7] D. J. Bammann, M. L. Chiesa, A. McDonald, W. A. Kawahara, J. J. Dike, and V. D. Revelli, "Prediction of Ductile Failure in Metal Structures," in: *Failure Criteria and Analysis in Dynamic Response*, ed. H. E. Lindberg, ASME AMD, vol. 107, 7 (1990).
- [8] L. Anand and W. Tong, "A Constitutive Model for Friction in Forming," *Annals of the CIRP*, vol. 42/1, 361 (1993).
- [9] P. A. Taylor, "CTH Reference Manual: The Bammann-Chiesa-Johnson Viscoplastic/Damage Model," Sandia National Laboratories report SAND96-1626 (1996).
- [10] A. T. Male and M. G. Cockcroft, "A Method for the Determination of the Coefficient of Friction of Metals under Conditions of Bulk Plastic Deformation," *J. Inst. Met.* **93**, 38 (1964-1965).

Intentionally Left Blank

Appendix A. Moving Subgrid Option

The CTH code has been modified to use separate domains (blocks) for various portions of a problem domain. This option is known as Multi-Block Communication (MBC). To increase the usefulness of this option it has been further modified to allow separate blocks to move relative to the main mesh. To achieve this, each block (a subgrid) is identified with one Lagrangian tracer point (see Figure A.1). As the material moves through the subgrid the tracer is moved at the material velocity. Once the tracer has moved more than 2 cells from its original position (the (I,J,K) position in the subgrid), the block is rezoned to place the tracer back at the original (I,J,K) site in the subgrid. This effectively causes the subgrid to move an integer number of cells widths whenever the tracer position exceeds the trigger criterion. This typically requires several computational cycles since material moves less (usually much less) than one cell width per computational cycle. It is important to note that the rezone step requires significantly more computational time than the usual cycle time, so not doing the rezone every cycle reduces the overall computation time. MBC also does a rezone each cycle, but only for the overlapping zones (where the block to block communication is accomplished).

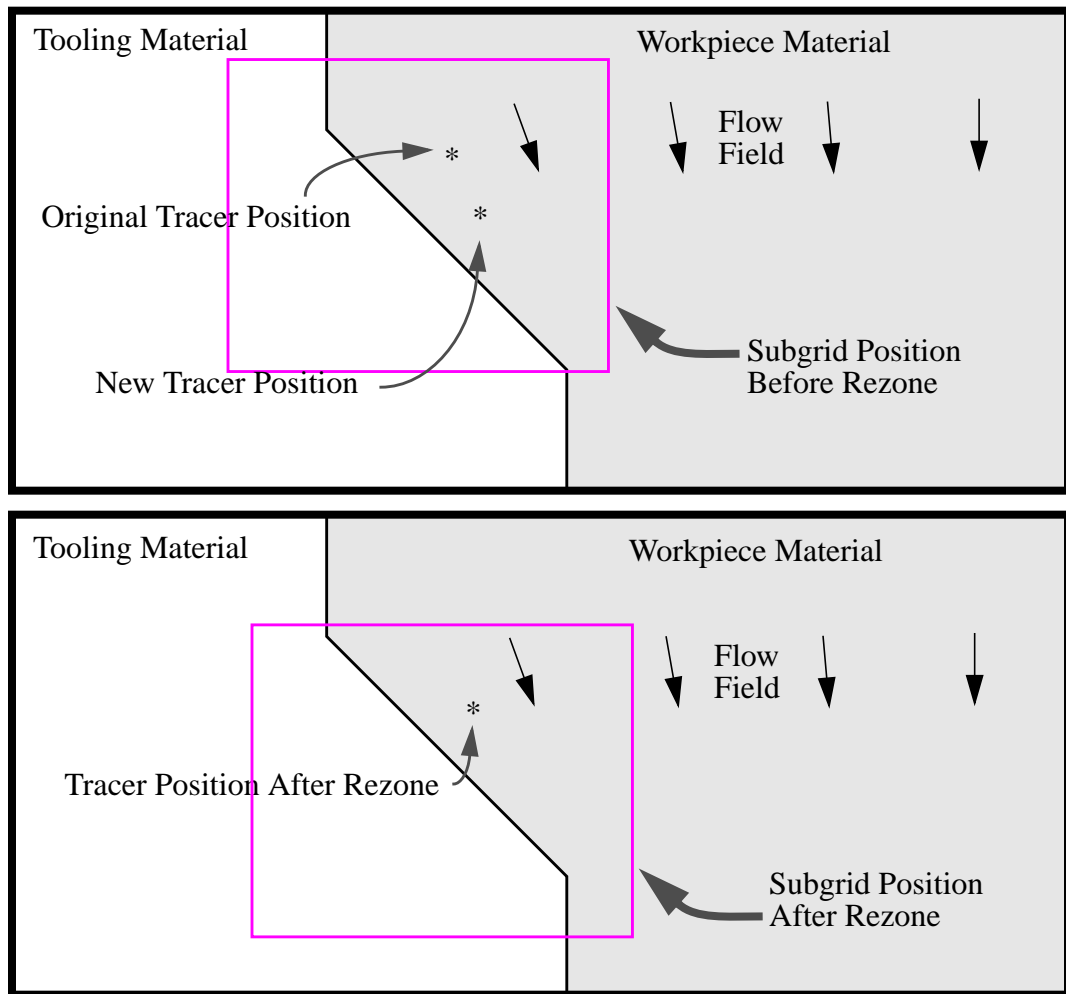


Figure A.1. Graphical representation of moving subgrid option.

Intentionally Left Blank

Appendix B. Dynamic Relaxation Algorithm

Dynamic relaxation (DR) is a technique for solving equilibrium or quasi-static problems in continuum and structural mechanics. To accomplish this, the DR scheme introduces a viscous damping term in the dynamic equations of motion to dissipate the kinetic energy of the system. To a great extent, DR is independent of the spatial discretization that is used. Thus it is applicable to finite difference codes, like traditional hydrocodes, as well as finite element codes with a variety of element types. Because DR uses explicit time integration, no technique for solving large sets of linear equations is necessary, and no matrix manipulations are required.

Because the essential features of DR are identical to those found in a typical solid dynamics code with explicit time integration, it lends itself to the modification of such a code to solve equilibrium or quasi-static problems. The purpose of this appendix is to provide a recipe for installation of DR in an existing solid dynamics code.

B.1 DR for Equilibrium Problems

After discretization of the equation of motion for a continuum or structure in a typical dynamic code, we have

$$M_i \frac{v_i^{n+1/2} - v_i^{n-1/2}}{\Delta t^n} = f_i^n + b_i^n, \quad (\text{B.1})$$

where i identifies a degree of freedom, n identifies a time step, Δt is the time step size, v is velocity, M is mass, b is the external force (from fields and boundary loads), and f is the resultant of all internal forces acting on the degree of freedom. For a code which uses a displacement variable, which we call u , we also have

$$v_i^{n+1/2} = \frac{u_i^{n+1} - u_i^n}{\Delta t^{n+1/2}}. \quad (\text{B.2})$$

To implement DR, we add a new term to the discretized equation of motion, eq.(B.1):

$$M_i \frac{v_i^{n+1/2} - v_i^{n-1/2}}{\Delta t^n} + \eta M_i \frac{v_i^{n+1/2} + v_i^{n-1/2}}{2} = f_i^n + b_i^n, \quad (\text{B.3})$$

where η is a damping coefficient, which we assume for the present purposes to be constant. The new term introduces viscous damping (not to be confused with artificial viscosity). Note that the damping term is centered in time at time step n , the same as the acceleration term. An alternative form is

$$M_i \frac{v_i^{n+1/2} - v_i^{n-1/2}}{\Delta t^n} + \eta M_i v_i^{n+1/2} = f_i^n + b_i^n, \quad (\text{B.4})$$

in which the damping term is centered instead at time step $n + 1/2$. In theory, the alternative form in eq.(B.4) is less accurate than eq.(B.3) because the terms are centered differently. In practice, this makes no difference, and we use eq.(B.4) as the basis for the remainder of this discussion.

Note that in any of eqs.(B.1), (B.3), or (B.4), the new velocity $v_i^{n+1/2}$ may be solved for immediately once the forces are known; thus DR does not change the fact that the method is explicit.

Suppose we are given a set of loads b_i , and we wish to find the solution to the equilibrium equations for a given body corresponding to these loads. At the start of a DR solution, we choose a convenient set of initial conditions. Normally, the initial state would be chosen so that the body is stress-free. We then apply the loads over time through a ramp function, while solving the altered equation of motion (B.4) at each time step. The effect of the viscous damping term in the equation of motion is to gradually remove all of the kinetic energy in the system (see Figure B.1). The iteration (i.e., the process of taking more time steps) is halted when some predetermined convergence condition is met. What is left is an approximation to the equilibrium solution to the problem. The application of loads and convergence conditions are discussed later in sections B.3 and B.4.

The damping coefficient η in eqs.(B.3) and (B.4) determines the rate of energy removal. For a given problem, there is an optimum value of η which results in the quickest rate of convergence. Unfortunately, in most cases, the optimum value cannot be determined in advance. In the most basic DR implementations, the damping coefficient η may be set by the user through input. An approximate method for choosing the optimum value is discussed later in section B.5.

B.2 DR for Quasi-static Problems

The difference between equilibrium and quasi-static problems is that in the former, there is no dependence at all on time. In the latter, there is a dependence on time, but the time evolution is so slow that the equation of equilibrium is an excellent approximation at any given time. So, in a quasi-static numerical simulation, we must retain a time variable, but at any given time we are solving the equations of equilibrium.

In quasi-static problems, the essential features of DR are unchanged from the previous section. However, we apply the method repeatedly to find solutions to the equilibrium equations at steps along the loading path.

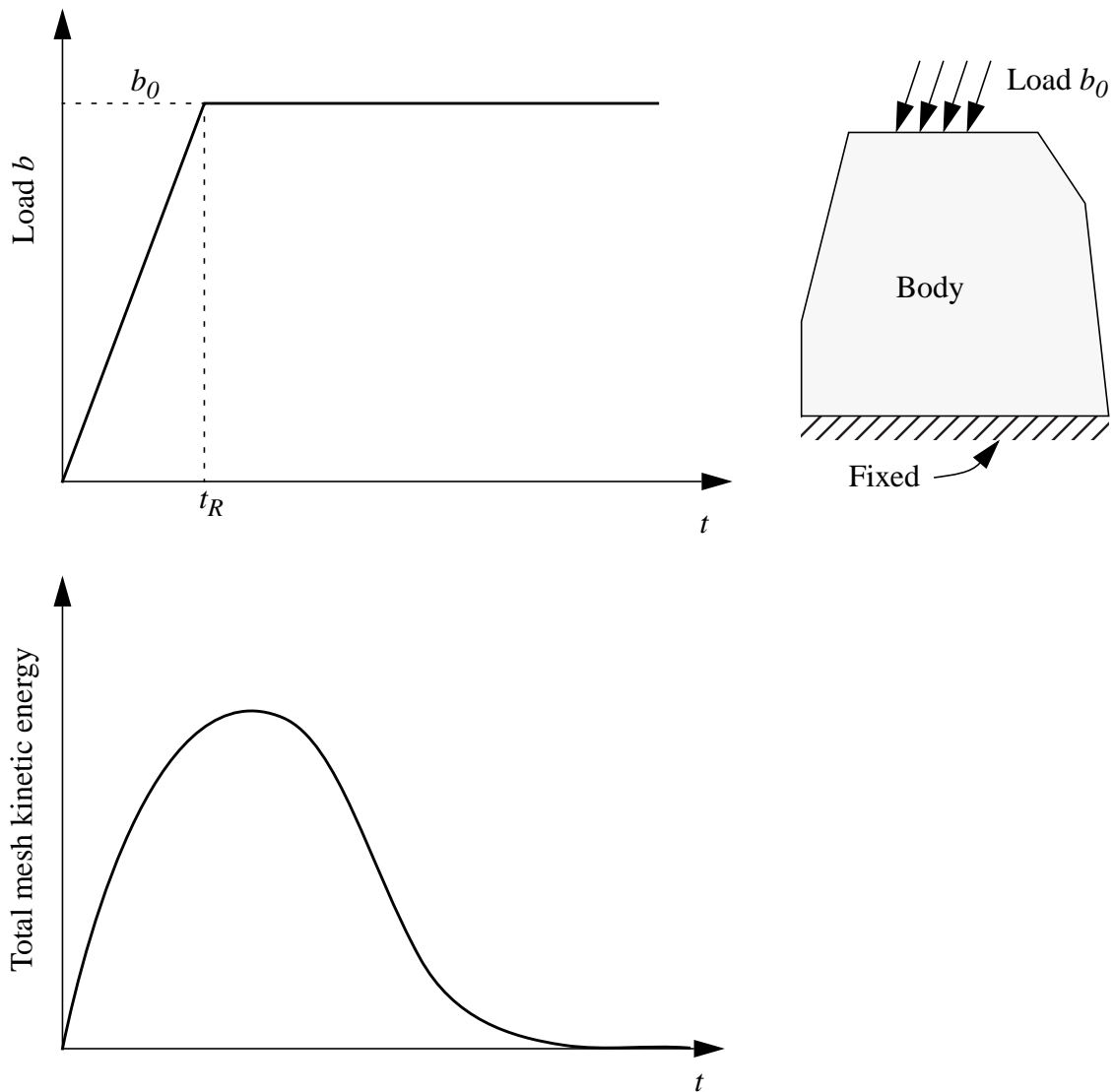


Figure B.1. Solution of an equilibrium problem by DR. Time evolutions of the load and the total kinetic energy of the mesh are shown.

We discretize the time interval to be simulated into equally spaced values T_0, T_1, T_2, \dots , where $T_0=0$ and the spacing is a constant ΔT . The value of ΔT is determined by the loading rate. If the load is applied over a time interval of 60 seconds, say, then a reasonable value of ΔT might be 1 second. We will call each point T_N along the loading path a *big time step*, and ΔT the *big time step size*.

In each big time step, we wish to find the equilibrium solution corresponding to the loads at the end of the time step, $b_0(T_N)$. To do this using DR, we ramp up the load $b(t)$ over a time scale that is small compared with ΔT but large compared with Δt , the time step controlled by the Courant-Friedrichs-Lewy stability condition (Figure B.2). We will call each point on the time axis t^n during the DR iteration the *little time step*, and Δt the *little time step size*.

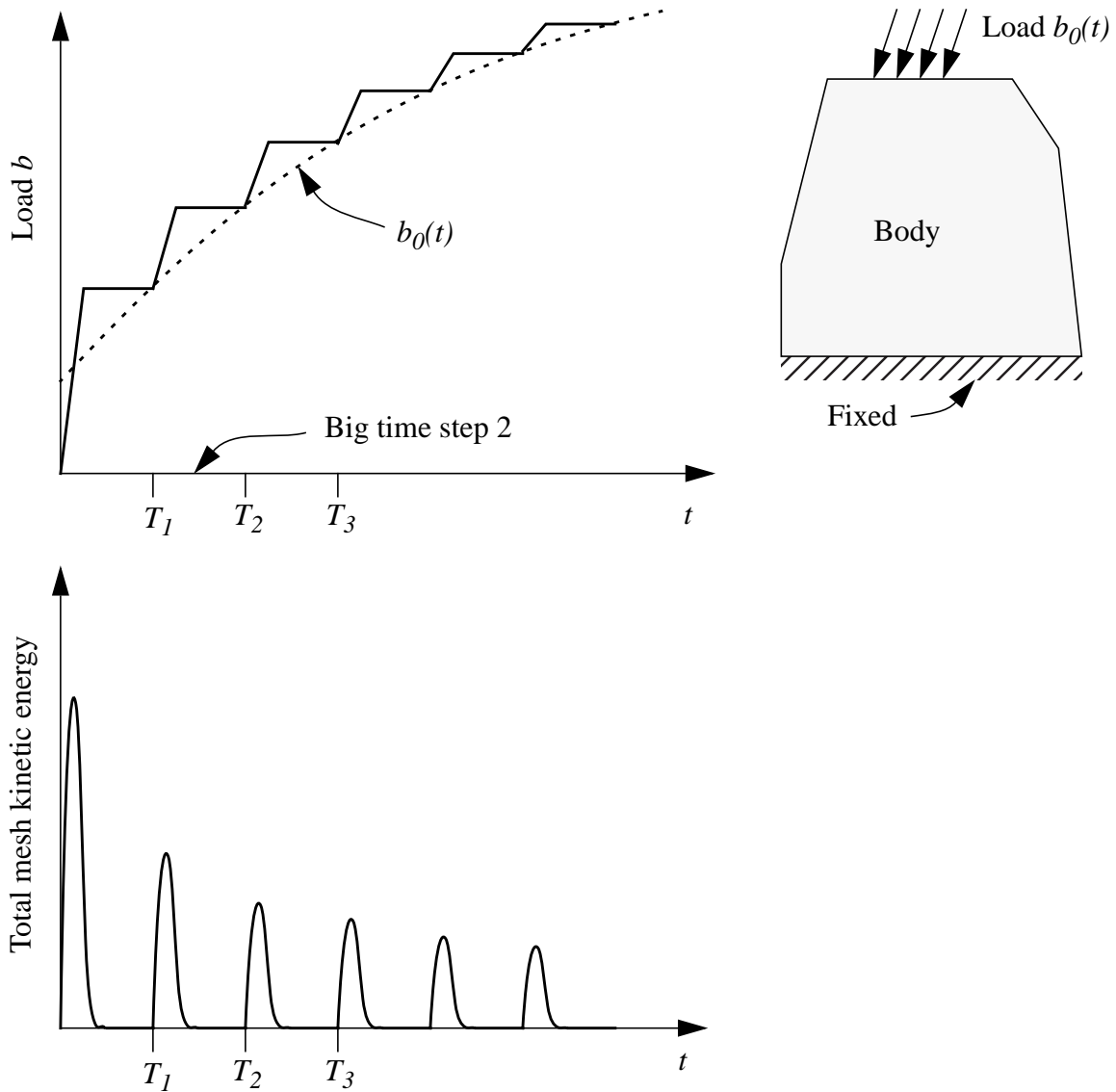


Figure B.2. Solution of a quasi-static problem by DR.

For example, a typical problem might require a little time step size $\Delta t = 10^{-7}$ seconds. Each DR iteration might require 500 little time steps to converge. It might at first appear that we would need 10,000,000 little time steps for each big time step. But after convergence, we know that the body is in equilibrium at the load prescribed at the end of the big time step, so there is no need for further calculation until the load changes again. So we omit the remaining 9,999,500 little time steps and go directly to the next big time step.

B.3 Application of Loads

From now on we will assume that the problem to be modeled is quasi-static. Equilibrium problems may be regarded as a special case of this with a single big time step.

At the start of each new big time step N , the load is ramped up over a time interval t_R to the value of the prescribed load at the end of the big time step, $b_0(T_N)$. The ramp time t_R is chosen keeping in mind the following trade-off:

- A small t_R is desirable because too large a value unnecessarily prolongs the iteration.
- The value of t_R must be large enough that the loading path followed by each material particle is similar to what it would experience in the actual quasi-static problem.

For example, suppose we are modeling a punch being forced at constant velocity into a block of elastic-plastic solid material. If $t_R = 0$, the problem in effect would be modeled as a series of hammer blows. This might give significantly different results than a larger value of t_R . Ideally, t_R should be greater than or equal to a few elastic wave transit times in the body being modeled.

B.4 Convergence Test

The most basic convergence test is as follows. Let V_{\max}^n be the maximum absolute value of any degree of freedom in the mesh at little time step n . Then we have convergence when

$$V_{\max}^n < V_{\text{tol}}, \quad (\text{B.5})$$

where V_{tol} is a user-defined tolerance.

In a problem in which the loads are applied through velocity or displacement boundary conditions, it is easy to determine a reasonable value for V_{tol} . It is simply a fraction of the boundary velocity that the mesh sees during the ramp loading. For example, suppose a punch moves at 0.001 m/sec, and $t_R/\Delta T = 10^{-5}$. Therefore, within the period of ramp loading, the mesh sees a boundary velocity of 100 m/sec. So, a reasonable convergence tolerance might be $V_{\text{tol}} = 5$ m/sec.

B.5 Choice of Damping Coefficient

It can be shown (see Underwood's article in [5]) that the optimum value of η is

$$\eta_{\text{opt}} = 2\omega_{\text{min}}, \quad (\text{B.6})$$

where ω_{min} is the lowest angular frequency of vibration of the mesh. Unfortunately, determining ω_{min} is a difficult problem in general.

It is, however, possible to find it exactly for some special cases. In particular, we consider the vibrational modes of a one-dimensional linear elastic rod of length L and wave speed c . The equation of motion in this case reduces to the one-dimensional wave equation,

$$\ddot{u} = c^2 u_{xx}. \quad (\text{B.7})$$

Using separation of variables, after applying the boundary conditions at the free ends

$u_x(0) = u_x(L) = 0$, we find that the solutions are of the form

$$u = \cos \frac{\omega x}{c} \cos \omega t, \quad \omega = \frac{m\pi c}{L}, \quad m = 1, 2, 3, \dots \quad (\text{B.8})$$

Therefore the lowest angular frequency is

$$\omega = \frac{\pi c}{L}. \quad (\text{B.9})$$

So, combining this result with eq.(B.6), the optimum damping coefficient is given by

$$\eta_{\text{opt}} = \frac{2\pi c}{L}. \quad (\text{B.10})$$

For more complex geometries, no such simple expression is obtainable. However, as a guess, we may use eq.(B.10) in the form

$$\eta_{\text{opt}} = \frac{2\pi \bar{c}}{\bar{L}}, \quad (\text{B.11})$$

where \bar{c} is an average elastic wave speed and \bar{L} is a characteristic length. For a continuous body, the characteristic length would be evaluated in the longest direction.

More accurate estimates of η_{opt} may be obtained for a given problem by trial and error. This may be worthwhile for a user to do if many large production runs are required for the same geometry.

Consequently, there should be two input options:

1. Input a value of \bar{L} and let the code determine \bar{c} and then η_{opt} from eq.(B.11).
2. Input a value of η .

B.6 Constitutive Modeling Issues

There is no change needed to typical equation of state or constitutive models when converting a code to DR, with the exception of models that use a strain rate (or other rate). The issue that arises with rate-dependent models is that during the DR iteration, because the changes in loads occur over a ramp time that is short compared with the big time step size, things change much faster than they do in the actual quasi-static problem. Therefore all the rates that are used by the model would be exaggerated unless we account for this effect in some way.

To do this, we make a slight modification to the rate-dependent constitutive model. Suppose we are concerned with a viscoplastic model which computes the flow stress Y according to

$$Y = f(\theta, \varepsilon, \dot{\varepsilon}), \quad (\text{B.12})$$

where θ is temperature, ε is strain, and f is a function. For a given cell or element, let the strain at little time step n be called ε^n , and let the strain at the end of big time step N be called E_N . In the unmodified dynamic code, we would compute the strain rate term in eq.(B.12) by

$$\dot{\varepsilon} \approx \frac{\varepsilon^n - \varepsilon^{n-1}}{\Delta t^{n-1/2}}. \quad (\text{B.13})$$

Now suppose instead that we are performing a quasi-static simulation using DR. We replace eq.(B.13) by

$$\dot{\varepsilon} \approx \frac{\varepsilon^n - E_{N-1}}{\Delta T}. \quad (\text{B.14})$$

Note that this modification requires the strain values from the previous big time step to be retained in an array.

B.7 Code Modification Steps

The following is a list of the steps needed to implement basic DR for quasi-static problems in an existing dynamic code:

1. Modify the equation of motion to include the damping term, eq.(B.4).
2. Create input parameters for t_R , ΔT , and \bar{L} or η .

3. Install the ramp boundary conditions.
4. Compute the maximum mesh velocity V_{\max}^n at the end of each little time step n . (It is a good idea to print out this value from time to time so the user can monitor how the iteration is progressing.)
5. Install the convergence test. When convergence is detected, the code should artificially increase the time to the next value of T_N .
6. Modify the rate terms in any rate-dependent equation of state or constitutive models as discussed above.

Distribution

1	MS 9405	D. J. Bammann, 8743
1	MS 9403	M. I. Baskes, 8712
1	MS 0321	W. J. Camp, 9200
1	MS 9042	M. L. Chiesa, 8743
1	MS 9403	D. A. Hughes, 8712
1	MS 9405	P. E. Nielan, 8743
1	MS 0820	S. A. Silling, 9232
20	MS 0820	P. A. Taylor, 9232
1	MS 0820	P. Yarrington, 9232
1	MS 0188	C. E. Meyers, 4523
1	MS 0188	Donna Chavez, 4523
1	MS 9018	Central Technical Files, 8940-2
5	MS 0899	Technical Library, 4916
2	MS 0619	Review & Approval Desk, 12690

For DOE/OSTI

